STUDY OF THE DISTRIBUTION OF DAILY FLUCTUATIONS IN OBSERVED SOLAR IRRADIANCES AND OTHER FULL DISK INDICES OF SOLAR ACTIVITY

JUDIT M. PAP

Jet Propulsion Laboratory, California Institute of Technology, MS 169-506, 4800 Oak Grove Dr., Pasadena, CA 91109, & Division of Astronomy and Astrophysics of the Department of Physics and Astronomy, University of California, Los Angeles, 405 Hilgard Ave., Los Angeles, CA 90095-1562, U.S.A.

ANNE VIGOUROUX

Laboratoire Cassini, associé au C.N.R.S. (U.R.A. 1362), Observatoire de la Côte d'Azur, B.P. 229, F-06304, NICE Cédex 04, FRANCE

and

PHILIPPE DELACHE*

Laboratoire Cassini, associé au C.N.R.S. (U.R.A. 1362), Observatoire de la Côte d'Azur, B.P. 229, F-06304, NICE Cédex 04, FRANCE

* Deceased on October 13, 1994

Abstract. Analyses based on irradiance observations from space within the last one and a half decades have discovered variations in the entire solar spectrum and at UV wavelengths on time scales of minutes to decades. In this paper we analyze the distribution of the measuring uncertainties and daily fluctuations in total solar irradiance measured by the Nimbus-7/ERB and SMM/ACRIM I radiometers as a function of solar cycle. Changes in solar total irradiance and its surrogates shorter than the solar rotation have also been considered as "noise" and have been removed from the data. Our results show that the noise (both instrumental and solar noise) changes as a function of the solar cycle, being higher during high solar activity conditions. The analysis of the scatter plot diagrams between the data and their standard deviation, the so-called "dispersion diagrams", provides a useful tool to estimate and predict the time of solar maximum and minimum activity conditions.

1. Introduction

For more than one and a half decades, solar irradiance (both bolometric and at different wavelengths) has been observed from different satellites. It has been shown that total solar and UV irradiances vary in parallel with the solar magnetic activity cycle, being higher during maximum solar activity conditions (e.g. Hudson, 1988). The long-term irradiance variations over the solar cycle are attributed to the changing emission of bright faculae and the magnetic network (e.g. Lean, 1987). The short-term irradiance changes (on the time scale of solar rotation) are directly related to the effect of active regions as they evolve and move across the solar disk (Lean, 1987) and to a lesser extent to the bright magnetic network (Pap, Marquette and Donnelly, 1991). Although considerable information exists on solar irradiance variability, the underlying physical mechanisms are not well understood as yet (see summary by Pap and White, 1994). Because of the lack of quantitative physical models of the solar radiative output, the current irradiance "models" have been developed with linear regression analysis, which provides only a general information about the observed irradiance changes. While there is a reasonably good agreement between measured total solar and UV irradiances and their regression estimates calculated from observations of dark sunspots, bright faculae and the magnetic network during the declining portion of solar cycle 21 and the rise of solar cycle 22, there is a breakdown between the observed and estimated irradiance values during maximum and minimum solar activity conditions.

It has been shown that the calculated total irradiance values underestimate the observed changes at the maximum of solar cycle 21 (Foukal and Lean, 1988; Willson and Hudson, 1991) and solar cycle 22 (Pap *et al.*, 1994; Brandt, Stix and Weinhardt, 1994). In the case of UV irradiance, the calculated irradiance values cannot account for the slow decrease in UV irradiance during solar minimum activity conditions (Donnelly, 1989; Barth *et al.*, 1990; Pap, London and Rottman, 1991). Furthermore, the "remaining part" of the irradiance power spectra after removing the effect of sunspots and bright magnetic features, including faculae, plages and the magnetic network, has peaks at periods of 9, 13.5, 27 and 300 days (Fröhlich and Pap, 1989; Pap and Fröhlich, 1992; Pap, 1992), and the amplitude of this residual variability depends on the phase of the solar cycle (Pap and Fröhlich, 1992).

It has not been clarified yet whether these discrepancies between the observed and calculated irradiance data are simply related to measuring uncertainties (in both irradiance and ground-based surrogates) or they characterize a real solar variability that may be related to global effects, such as large scale motions (Ribes, Mein and Mangeney, 1985), radius changes (Ulrich and Bertello, 1995) and/or photospheric temperature changes (Kuhn, Libbrecht and Dicke, 1988). Considering that the radiative output of the Sun is the main driver of the physical processes in the Earth's atmosphere and its climate system, this problem has become one of the most important issues in solar-terrestrial physics.

The main objective of this paper is to (1) separate the observational uncertainties and physical fluctuations in total solar irradiance and (2) determine the amplitude of the real fluctuations in the examined time series over the solar cycle. In order to interpret the results gained from various types of statistical analyses, it is essential to understand and evaluate the uncertainties in the data. Identification of random fluctuations in the data sets provide an important clue to estimate the signal-to-noise ratio and to clarify whether the observed small residual variability in solar irradiance is simply determined by a noise component in the data or whether it clearly represents a real solar variability. The corresponding results on the distribution of daily fluctuations (related to both instrumental and solar noise) of solar irradiance and its ground-based surrogates are described in this paper.

2. Description of the data

Total solar irradiance, the integrated solar flux over the entire solar spectrum, has been measured from space for over a decade. The direct space observations of total solar irradiance began in late November of 1978 by the Earth Radiation Budget (ERB) experiment on board the Nimbus-7 satellite that was terminated in January of 1993 (Kyle *et al.*, 1993). The ERB experiment was a multipurpose experiment that included an electrically self-calibrating active cavity radiometer with an estimated at-launch accuracy of $\pm 0.5\%$ (Hickey *et al.*, 1988). Limitations imposed on the ERB solar observations by the absence of solar pointing on the Nimbus platform sustained a noise level in the ERB results which was estimated as $\pm 0.03\%$ (Hoyt *et al.*, 1992) and this low precision inhibited the recognition of intrinsic solar variability until subsequent detection by the Active Cavity Radiometer Irradiance Monitoring (ACRIM) experiment on board the SMM satellite (Willson *et al.*, 1981). The irradiance observations of the SMM/ACRIM radiometer started in February 1980. During the first 10 months of the ACRIM observations the measuring precision was so high ($\pm 0.002\%$) that each observed event had a solar, rather than an instrumental, origin (Willson, 1984). The high precision and accuracy of the ACRIM I observations are attributed to the phased operation of its three independent ACR sensors and the full time solar pointing of the SMM satellite (Willson and Hudson, 1991). Unfortunately, in December 1980 the solar-pointing system of the SMM satellite failed and it was placed into the so-called "spin-mode". During this operational mode until May 1984, when the SMM was repaired during a Space Shuttle Mission, the measuring precision decreased by about a factor of 5 (from 0.002% to 0.01%) (Willson, 1984). After May 1984 the original measuring precision was restored and the original high quality ACRIM I total irradiance data were collected through November 1989 when the operation of the SMM satellite was terminated.

Extensive measurements of the solar ultraviolet irradiance have been made by the Solar Backscatter Ultraviolet (SBUV1) experiment on the Nimbus-7 satellite between 160–400 nm from November 1978 through 1987 (Schlesinger and Cebula, 1992; Cebula, Hilsenrath and Deland, 1994) and by the NOAA9 and NOAA11/SBUV2 instruments since 1985 (Donnelly, 1991; Donnelly, White and Livingston, 1994). Although the SBUV experiments suffer from a significant degradation in its diffuser reflectivity, the ratio of the irradiance in the core of the Mg 280 nm line to the irradiance at the neighboring continuum wavelengths (Mg II h & k core-to-wing ratio) can be used as an index of solar variability (Heath and Schlesinger, 1986). It has been demonstrated that the Mg II index is capable of measuring solar rotational modulation on both 27 and 13.5 days time scales and solar cycle variability on the 11-year time scale (Donnelly and Puga, 1990; Pap, Tobiska and Bouwer, 1990). Since the UV irradiance plays a significant role in the dynamics of the middle atmosphere of the Earth and establishing its chemical composition through photodissociation and photoionization processes, it is highly desirable to develop a proxy indicator for these variations. Heath and Schlesinger (1986) have derived "scale factors" to relate the Mg II index variations to changes at other UV wavelengths. The Nimbus-7 and NOAA9 Mg core-to-wing ratios (Mg c/w) were made consistent by means of their overlapping observational time period in 1986, and also by means of the full disk Ca II K index (Donnelly, 1991; Donnelly, White and Livingston, 1994). Two sets of the Mg c/w index have been available, derived at The NASA/Goddard Space Flight Center (GSFC) (Cebula, Hilsenrath, and Deland, 1994) and at the NOAA/Space Environment Laboratory (SEL) (Donnelly, White, and Livingston, 1994), respectively. In this paper the NOAA/SEL Mg c/w ratio has been used as a measure of UV irradiance.

In order to directly compare the variations in total solar irradiance with the changes in the UV irradiance at 280 nm represented by the Mg c/w, the effect of sunspots have been removed from total irradiance by means of the Photometric Sunspot Index (Hudson *et al.*, 1982; Fröhlich, Pap and Hudson, 1994). The Photometric Sunspot Index (PSI) relates the observed sunspot areas and their contrast to a net effect on the radiative output of the observed solar hemisphere and it is corrected for the photospheric limb darkening. The original PSI function (Hudson *et al.*, 1982) was calculated on the assumption that the area and temperature ratio of the umbra and penumbra are constant and therefore the PSI function was calculated on the basis of a constant contrast value of sunspots (details on the calculation of PSI are given by Hudson et al., 1982 and Fröhlich, Pap and Hudson, 1994). However, results of the photometry of sunspots have demonstrated that the contrast of sunspots is not a constant value: it changes as a function of their area (Steinegger *et al.*, 1990) and the solar cycle (Maltby *et al.*, 1986). Based on the results of photographic photometry published by Steinegger *et al.* (1990), the PSI function, used in this study, has been recalculated by Fröhlich, Pap and Hudson (1994). Since the solar magnetic activity is assumed to be the driving force for irradiance variability (e.g. Harvey, 1994), the full disk magnetic flux measured at the National Solar Observatory at Kitt Peak is included in our analysis and it has been directly compared to the irradiance data.

3. Time series and their uncertainties

3.1. Study the daily standard deviations of total solar irradiance

The SMM/ACRIM I daily mean values with their standard deviations (thereafter STD) are plotted in Figure 1a for the time interval of 1980 to 1989. The vertical error bars in Figure 1a indicate the standard deviations of the mean of the irradiance samples obtained within a day. To study the relation between the data and their uncertainty, the STD of the SMM/ACRIM I data versus their daily means are presented in Figure 1b. As can be seen from Figure 1a, total solar irradiance continuously decreased from the maximum of solar cycle 21 (1980) towards solar minimum and started to rise in early 1987 with the ascending phase of solar cycle 22 (Willson and Hudson, 1988). The increased measuring uncertainty during the spin operational mode of the SMM satellite is clearly seen in Figure 1a. In order to study the variability of STD in more detail, the normal operational and spin-mode data have been separated and their STD has been plotted against the daily mean values in Figures 2a,b, respectively. While no particular structure can be seen in the case of the spin-mode data (Figure 2b), the ACRIM I data during the normal operational mode (Figure 2a) form a certain pattern on the scatter plot diagram of their standard deviation. Most of the irradiance values

(95%) are concentrated below 0.05 W/m^2 STD, whereas the outliers from that main cluster (STD>0.05) tend to be distributed around two vertical lines.

To further investigate the physical nature of the pattern observed in the normal mode of ACRIM I data, the quiet- and active-Sun irradiance values and their standard deviations have been separated. The quiet-Sun irradiance values have been choosen for the time interval of July 1, 1984 to September 30, 1986, when total solar irradiance showed only a small variability around its mean value. There was an obvious decline in solar activity in July 1984 and after this time only small sunspots occurred on the Sun. Although the magnetic solar minimum occurred in September 1986, in October large active regions, already belonging to solar cycle 22, were formed on the Sun and caused significant variability in both UV and total solar irradiances (Pap, Marquette and Donnelly, 1991). Irradiance values between February and December 1980 and after October 1, 1986 have been identified as active-Sun values in this phase of our study.

The scatter plot diagram of the quiet-Sun irradiance values and their standard deviations are presented in Figure 3a. The vertical line represents the mean value of the quiet-Sun irradiance (1367.07 W/m^2). Figure 3b consists of a particular part of the quiet-Sun data with STD smaller than 0.06 W/m^2. Most of these data points ($\sim$74%) are concentrated between STD 0.004 and 0.005 W/m^2 and these numbers essentially represent the intrinsic precision of the ACRIM I data (corresponding to 0.0004%), in a good agreement with the published value for the average uncertainty of the ACRIM I data (better than $\pm$0.002%; Willson, 1984). The structures seen in Figures 3a,b represent a Gaussian distribution of the data around their mean value. Since during solar minimum only small variability is observed in total irradiance, data points above 0.01 W/m^2 STD represent the random noise in the data. The active-Sun values and the corresponding standard deviations are plotted in Figure 3c and these data show a very similar pattern to that seen in Figure 2a (data points plotted for the whole normal operational time interval). Namely, data points with STD larger than 0.05 are again distributed around two vertical lines. The first vertical line is drawn at the mean irradiance value (M = 1367.36 W/m^2) for the rising portion of solar cycle 22 between October 1, 1986 and June 2, 1989, the end of the ACRIM I data set. The second vertical line represents the mean irradiance value for the maximum of solar cycle 21 in 1980 (M = 1368.35 W/m^2). These two distributions represent most closely Gaussian distributions and these data (STD>0.05) can again be regarded as random fluctuations in the data.

Another interesting feature of Figures 2 and 3 is that the standard deviation less than 0.05 W/m^2 increases with the increasing daily mean values of total irradiance from minimum to maximum activity conditions. The higher irradiance values represent maximum solar activity conditions (Willson and

Hudson, 1988; Foukal and Lean, 1988), when significant changes may occur within a day due to the effect of flares as well as the formation and evolution of active regions, especially sunspots. In contrast, during minimum activity conditions, when only a few and small active regions occur on the Sun, variations in total solar irradiance within a day are small, and this may explain the lower standard deviation of the ACRIM I total solar irradiance values during solar minimum.

The daily Nimbus-7/ERB irradiance values with their standard deviations are presented in Figure 4a. The ERB STD values versus the daily means are shown in Figure 4b. As can be seen from Figure 4, the uncertainty of the Nimbus data is much higher than that of the ACRIM I data (except for the spin-mode ACRIM I data) due to the lack of a solar pointing platform and the limited number of observations (Hickey *et al.*, 1988). While in the case of the normal operation of the ACRIM experiment more than 800 observations were taken within a day (Willson, 1984), the ERB experiment had a 3-day-on and 1-day-off operational mode through most of its operation and the number of observations was limited to less than a dozen per day (Hickey *et al.*, 1988). The Nimbus-7/ERB irradiance values do not show the pattern seen in the case of the normal mode of ACRIM data, instead they form a large cloud and the data are evenly distributed between STD = 0.05 and 0.5 similar to the spin-mode ACRIM I data. Figure 4c represents the distribution of the quiet-Sun ERB values (for the same time interval as choosen for the ACRIM I data). Although higher irradiance values represent maximum activity conditions similar to the ACRIM I observations, the Gaussian distribution, that was clearly seen in the case of the normal mode of ACRIM I data, is not recognized in the ERB data because of their larger uncertainty. The mean STD values for both the ERB and ACRIM I total irradiance during the quiet- and active-Sun conditions are listed in Table I. Table I also contains the maximum, minimum and mean quiet- and active-Sun irradiance values as well as the number of the corresponding data points.

3.2. Study of the monthly dispersion of the data

Since we are especially interested in the long-term irradiance variability and its relation to solar magnetic activity, any changes shorter than the solar rotational period have been considered as “noise” and removed from the data by calculating monthly averages in a similar way as published by Vigouroux and Delache (1994). This uncertainty of the monthly averages, called dispersion (DISP), is calculated from the corresponding daily values, analogue to the calculations of the STD standard deviations:

$$DISP = \sqrt{\frac{\sum (D_i - \bar{D})^2}{n-1}}$$

where D_i represents the daily data within 30 days and $\bar{D}$ their 30-day mean.

According to the definition of the dispersion, its value represents the monthly variability of the data. The dispersion values versus the monthly total irradiance averages are plotted in Figure 5, where the quite-Sun values are represented by crosses and the active-Sun values by dots. Note that only the ACRIM I data have been used in the discussions to follow since they provide a more accurate measure of the total solar energy flux than the Nimbus-7/ERB irradiance values. The dispersion values were also calculated for the spin-mode data since the monthly averages smooth out the large daily fluctuations partly arising from measuring uncertainties related to the lack of proper solar pointing.

As can be seen, the dispersion values are higher during active-Sun conditions, similar to the scatter plot diagrams of the STD and ACRIM I daily irradiance values presented in Figure 2a and Figure 3c. Since in this case the "uncertainty", the calculated dispersion, means real solar variability, this confirms that the higher standard deviation of the ACRIM I data during higher solar activity is related more to solar effects than to instrumental uncertainties. Although the crosses, representing solar minimum activity values, are concentrated around the 1367 W/m^2 minimum irradiance value, the difference between their maximum and minimum values exceeds 0.5 W/m^2 (note that the full range of the observed solar cycle variability in the monthly averages of ACRIM total irradiance is about 1.8 W/m^2). To further examine the change of the dispersion over the solar cycle and to establish the real time of solar minimum for total solar irradiance, the dispersion diagrams have been plotted on a yearly basis (Figure 6).

As can be seen from Figure 6, there is an obvious pattern in the ACRIM I dispersion diagrams and this pattern changes as a function of the solar cycle. During solar minimum the dispersion values form a concentrated cluster of data, this feature is the most pronounced during 1986. It is interesting to note that towards maximum activity conditions this cluster is less and less compressed and the variability within the cluster shows a larger range between 0.5 and 1.4 W/m^2. Since the dispersion represents the daily fluctuation around the monthly mean value of the particular solar index, the variation within a particular cluster is related to the short-term variations, presumably due to aggregate fluctuation in radiances from all surface structures seen on the visible solar disk. Therefore, study of the shape and rate of compression of the dispersion clusters may provide an additional and useful tool to estimate and predict the time of maximum and minimum solar activity conditions for solar total and UV irradiances at various wavelengths as well as for additional solar parameters.

The dispersion values have also been calculated for the Mg c/w, PSI and magnetic flux values to clarify whether the cluster structure found in the case of the ACRIM data is a general pattern for other solar indices. To directly compare the temporal variation of total solar irradiance and the Mg c/w ratio, the effect of sunspots has been removed from total irradiance by means of the PSI function. The time series of total irradiance corrected for sunspot darkening (S_c = ACRIM I + PSI), the Mg c/w ratio, PSI and the full disk magnetic flux are presented in Figures 7(a) to (d). It is interesting to note that while the maximum activity level for the Mg c/w ratio is almost identical during solar cycles 21 and 22, the strength of the magnetic flux is much higher during the maximum of cycle 22 than during cycle 21. An additional difference is obvious from these time series: the Mg c/w ratio reaches maximum activity values before the magnetic flux during both solar cycles. In addition, both Mg c/w ratio and total irradiance corrected for sunspot darkening start to rise prior to the magnetic flux at the beginning of the ascending phase of solar cycle 22.

The yearly dispersion diagrams of the Mg c/w ratio from 1979 to 1994 are presented in Figures 8 and 9. As can be seen, the dispersion of the Mg c/w data also forms a cluster structure, similar to total irradiance. It is interesting to note that between 1979 and 1981 the shape of these clusters is almost vertical and the data points fluctuate around 0.28. This structure demonstrates that the Mg c/w had about a 3-year-long flat maximum variability during solar cycle 21. The dispersion cluster started to move toward lower Mg c/w values in 1982, although the extended shape of the cluster indicates that the short-term variability still was significant at the beginning of the declining phase of solar cycle 21. The dispersion clusters had become more compressed by 1984, however these clusters were never as compressed as the ones for total irradiance during minimum activity conditions. This feature indicates that the short-term variability in UV irradiance at 280 nm (Mg c/w) is significantly higher during minimum activity condition than in the total solar flux. These dispersion diagrams place the minimum time of the Mg c/w ratio in 1985 and 1986, and as can be seen from Figure 8, a slight increase in the Mg c/w started in 1987. The pattern in the dispersion diagrams for 1989 to 1991 (see Figure 9) was very similar to that of the maximum of cycle 21, demonstrating that the two maxima of solar cycles 21 and 22 were almost identical in the case of the Mg c/w. The dispersion diagram for 1992 shows that a sudden decrease in the Mg c/w ratio occurred during this period and the amplitude of this decrease was as large as that of the observed decline between early 1982 and the end of 1983. This sudden decrease in the Mg c/w ratio (and at other UV wavelengths) happened between February and June of 1992 (White et al., 1994) and was caused by the disappearance of the magnetic activity in the southern solar hemisphere (Harvey, 1994).

We note that similar clusters have been found in the Nimbus-7/ERB total irradiance, the PSI and the full disk magnetic flux, indicating that the dispersion diagrams provide a helpful tool in studying long-term changes in various solar activity indices. In the discussion to follow we will examine the dispersion diagrams during minimum solar activity conditions to better estimate the minimum time of solar total irradiance, the Mg c/w ratio and the measures of the solar magnetic activity. Figure 10 shows the dispersion diagrams for the ACRIM I total irradiance (a), S_c (b), Mg c/w (c), PSI (d), and the magnetic flux (e). The dots represent data for 1984, crosses for 1985, diamonds for 1986, and stars for 1987. As the distribution of the dots (data for 1984) shows in Figure 10, part of 1984 belonged to the declining portion of solar cycle 21. The beginning of the minimum of solar cycle 21 has been determined for each data set by studying the distribution of the dots on a monthly basis. The ending date of solar minimum has been determined in a similar fashion: the distribution of stars (representing data points for 1987) made it possible to determine whether these data belonged to the cluster of minimum activity values. The estimated solar minimum intervals (beginning and ending dates) and the length of the minimum of solar cycle 21 for solar total irradiance, the Mg c/w ratio as well as for the magnetic surrogates are listed in Table II. As can be seen from Table II, the length of solar minimum is much shorter in the case of solar total and UV irradiance at 280 nm than in the case of solar indices representing strong magnetic field, such as the full disk magnetic flux and PSI.

Figures 11(a)-(e) show the dispersion diagrams of the ACRIM I (a), S_c (b), Mg c/w (c), PSI (d), and the magnetic flux (e), including both quiet- and active-Sun values. The crosses on each plot represent the minimum activity conditions for the time intervals shown in Table II and the dots indicate the active-Sun values including data for maximum solar activity conditions as well as for the decline and rise of solar cycles 21 and 22. Note that the investigated time series cover different time intervals and this does not allow a detailed analysis of the dispersion diagrams for maximum solar activity. This is especially true for total solar irradiance, for which there are no high precision observations covering the whole time interval of the maxima of solar cycles 21 and 22.

As can be seen from Figures 11(a)-(e), the relation between the dispersion and the monthly averages of the data is quite different for solar minimum and active-Sun conditions. In the case of solar irradiance (both bolometric and the UV flux at 280 nm) as well as the magnetic flux data, the minimum values are concentrated along almost a vertical line indicating the fluctuations of these data around their mean at the time of solar minimum. In contrast, in the case of the PSI function the regression lines for both quiet- and active-Sun conditions converge towards zero because the value of PSI is always zero in the absence of sunspots, independent of the phase of the solar activity cycle. Another interesting feature can be recognized in these dispersion diagrams, namely the scatter of the data is much larger for higher data values. This arises from the larger variability in the data during solar maximum due to the changes on active region time scales. This feature is most obvious in the case of the Mg c/w. The distribution of the maximum values of the Mg c/w ratio is related to the several years long maximum activity of both solar cycles 21 and 22, as has already been seen in Figure 6.

4. Conclusions

In this paper we have applied a new method, following the original idea of Vigouroux and Delache (1994), to evaluate and understand the uncertainties in solar total and UV irradiance at 280 nm represented by the Mg c/w ratio, and magnetic activity indices, such as the PSI function and the full disk magnetic flux. It has been shown that study of the scatter plot diagrams between daily solar irradiance measurements and their standard deviations provides an important tool to separate the random fluctuations related to instrumental effects from real solar variations.

Our results show that the standard deviations of total solar irradiance depend on the phase of the solar cycle. We have found that the values of the standard deviations in the case of the Nimbus-7/ERB and SMM/ACRIM I total irradiances are larger during maximum solar activity conditions. In contrast, during solar minimum the standard deviations are small and their scatter represents the intrinsic precision of the measurements. The larger values of the standard deviations of total irradiance during solar maximum are attributed to the large daily irradiance fluctuations related to the evolution of active regions.

Our results show that the dispersion diagrams of total irradiance and its surrogates provide a new approach to study the long-term changes over the solar cycle. A cluster structure of these diagrams has been discovered and it is shown that the shape and the compression of these clusters change as a function of the solar cycle. These investigations may provide an important new technique in predicting the time behavior of solar activity indices and estimating the occurrence of the maximum and minimum of solar cycle.

Our results indicate that the length of the solar minimum is different for solar total irradiance and for the Mg c/w proxy of UV irradiance and various measures of solar magnetic activity, such as the full disk integrated magnetic flux and the Photometric Sunspot Index. It has been shown that there is a phase shift between the changes in the solar magnetic flux and solar irradiance at the beginning and the end of solar minimum. In addition, both total solar and UV irradiances start to rise about 8 to 10 months prior to the magnetic flux and PSI at the beginning of the ascending phase of solar cycle 22. The origin of this phase shift is not yet understood. It is an open question whether the current magnetic field measurements cannot recognize faint solar features, such as the network and intranetwork elements, or the discovered phase shift is related to non-linear coupling between the subphotospheric, photospheric and chromospheric layers.

Acknowledgements

The research described in this paper was carried out by the Jet Propulsion Laboratory, California Institute of Technology and University of California, Los Angeles, under a contract with the National Aeronautics and Space Administration (J.M. Pap) and by the laboratoire Cassini, associé au C.N.R.S. (U.R.A. 1362) of the Observatoire de la Côte d'Azur (A. Vigouroux). The SMM/ACRIM I data used in this study have been produced by the Active Cavity Radiometer Irradiance Monitoring Group at JPL. The Nimbus-7/ERB data were kindly provided by Dr. D. Hoyt. We acknowledge the NASA/GSFC Ozone Processing Team (OPT) for the Nimbus-7 SBUV/1 data and NOAA/NESDIS for the SBUV/2 data, which were kindly provided by L. Puga. The NSO/Kitt Peak magnetic data used here are produced cooperatively by NSF/NOAO, NASA/GSFC and NOAA/SEL and provided by courtesy of Dr. J. Harvey. The useful comments of Drs. R.F. Donnelly, E. Fossat, M. Neugebauer, L. Puga as well as an unknown referee are highly appreciated.

References

Barth, C.A., Tobiska, K. , Rottman, G.A. and White, O.R.: 1990, *Geophys. Res. Lett.* **17**, 571.

Brandt, P.N., Stix, M. and Weinhardt, H.: 1994, *Solar Phys.* **152**, 119.

Cebula, R.P., Hilsenrath, E. and Deland, M.T.: 1994, in *The Sun as a Variable Star: Solar and Stellar Irradiance Variations* (eds. J.M. Pap, C. Fröhlich, H.S. Hudson, and S.K. Solanki), Cambridge Univ. Press., 81.

Donnelly, R.F.: 1989, *Handbook*, for MAP (eds. J. Lastovicka, T. Miles, and A. O'Neill) **29**, 1.

Donnelly, R.F. and Puga, L: 1990, *Solar Phys.* **130**, 369.

Donnelly, R.F.: 1991, *J. Geomagnet. Geoelect.* **43 Suppl.**, 835.

Donnelly, R.F., White O.R. and Livingston, W.C.: 1994, *Solar Phys.* **152**, 69.

Foukal, P. and Lean, J.: 1988, *Ap.J.* **328**, 347.

Fröhlich, C. and Pap, J.: 1989, *Astron. Astrophys.* **220**, 272.

Fröhlich, C., Pap, J. and Hudson, H.S.: 1994, *Solar Phys.* **152**, 111.

Harvey, K.: 1994, in *The Sun as a Variable Star: Solar and Stellar Irradiance Variations* (eds. J.M. Pap, C. Fröhlich, H.S. Hudson, and S.K. Solanki), Cambridge Univ. Press., 217.

Heath, D. F. and Schlesinger, B.M.: 1986, *J. Geophys. Res.* **91**, 8672.

Hickey, J.R., Alton, B.M., Kyle, H.L. and Hoyt, D.V.: 1988, *Space Sci. Rev.* **48**, 321.

Hoyt, D.V., Kyle, H.L., Hickey, J.R. and Maschhoff, R.H.: 1992, *J. Geophys. Res.* **97**, 51.

Hudson, H.S.: 1988, *Ann. Revs. Astron. Astrophys.* **26**, 473.

Hudson, H.S., Silva, S., Woodard, M. and Willson, R.C.: 1982, *Solar Phys.* **76**, 211.

Kuhn, J., Libbrecht, K.G. and Dicke, R.: 1988, *Science* **242**, 908.

Kyle, H.L., Hoyt, D.V., Hickey, J.R., Maschhoff, R.H. and Vallete, B.J.: 1993, *NASA Reference Publ. 1316*, GSFC, Greenbelt.

Lean, J.: 1987, *J. Geophys. Res.* **92**, 839.

Maltby, P., Carlsson, M., Kjeldseth-Moe, O., Avrett, E.H., Kurucz, R.L.: 1986, *Ap.J.* **306**, 284.

Pap, J.: 1992, *Astron. Astrophys.* **264**, 249.

Pap, J. and Fröhlich, C.: 1992, in *Proc. Solar Electromagnetic Radiation Study for Solar Cycle 22*, (eds. R.F. Donnelly), SEL, NOAA/ERL, Boulder, 62.

Pap, J. and White, O.R.: 1994, in *Proc. of NATO Advance Research Workshop on the Solar Engine and its Influence on Terrestrial Atmosphere and Climate*, (eds. E. Ribes), NATO ASI Series, vol. I 25, Springer-Verlag, 235.

Pap, J., Marquette, W.H. and Donnelly, R.F.: 1991, *Adv. Space Res.* **11**, 271.

Pap, J., Tobiska, K. and Bouwer, D.: 1990, *Solar Phys.* **129**, 165.

Pap, J., London, J. and Rottman, G.A.: 1991, *Astron. Astrophys.* **245**, 648.

Pap, J., Willson, R.C., Fröhlich, C., Donnelly, R.F. and Puga, L.: 1994, *Solar Phys.* **152**, 13.

Ribes, E., Mein, P. and Mangeney, A.: 1985, *Nature* **318**, 170.

Schlesinger, B.M. and Cebula, R.P.: 1992, *J. Geophys. Res.* **97**, 10119.

Steinegger, M., Brandt, P., Pap, J. and Schmidt, W.: 1990, *Astrophys. Space Sci.* **170**, 127.

Ulrich, R. and Bertello, L.: 1995, *Nature* **377**, 214.

White, O.R., Rottman, G.J., Woods, T., Knapp, B.G.,Keil, S., Livingston, W.C., Tapping, K.F., Donnelly, R.F. and Puga, L.: 1994, *J. Geophys. Res.* **99**, 369.

Vigouroux, A. and Delache, Ph.: 1994, *Solar Phys.* **152**, 267.

Willson, R.C.: 1984, *Space Sci. Rev.* **38**, 203.

Willson, R.C. and Hudson, H.S.: 1988, *Nature* **332**, 810.

Willson, R.C. and Hudson, H.S.: 1991, *Nature* **351**, 42.

Willson R.C., Gulkis, S., Janssen, M., Hudson, H.S. and Chapman, G.A.: 1981, *Science* **211**, 700.

data	min irrad	max irrad	mean irrad	mean STD	nb points
ACRIM I					
all	1364.479	1369.709	1367.501	0.047	3052
spin-mode	1364.479	1369.526	1367.730	0.104	1018
normal-mode	1365.219	1369.709	1367.387	0.018	2034
active Sun	1365.219	1369.709	1367.577	0.024	1262
quiet Sun	1366.290	1367.672	1367.075	0.009	771
Nimbus					
all	1368.57	1374.88	1372.07	0.16	4515
active Sun	1368.57	1374.88	1372.20	0.16	3723
quiet Sun	1370.67	1372.11	1371.47	0.15	792

TABLE I
The minimum, maximum and mean irradiance values for the SMM/ACRIM I and Nimbus-7/ERB irradiance values are listed together with the mean standard deviation and number of data points for the whole observing time intervals as well as for the quiet- and active-Sun periods.

Time Series	Beginning of Minimum	End of Minimum	Length
ACRIM I	January 1985	August 1987	32 months
ACRIM I + PSI	January 1985	March 1987	27 months
PSI	August 1984	October 1987	39 months
Mg c/w	January 1985	March 1987	27 months
Magn. field	August 1984	December 1987	41 months

TABLE II

The beginning and ending dates of minimum solar activity conditions during solar cycle 21 for the investigated time series. These dates were estimated from analyzing the time series as well as from the dispersion diagrams presented in Figure 10. The length of the estimated solar minimum is also given in months.

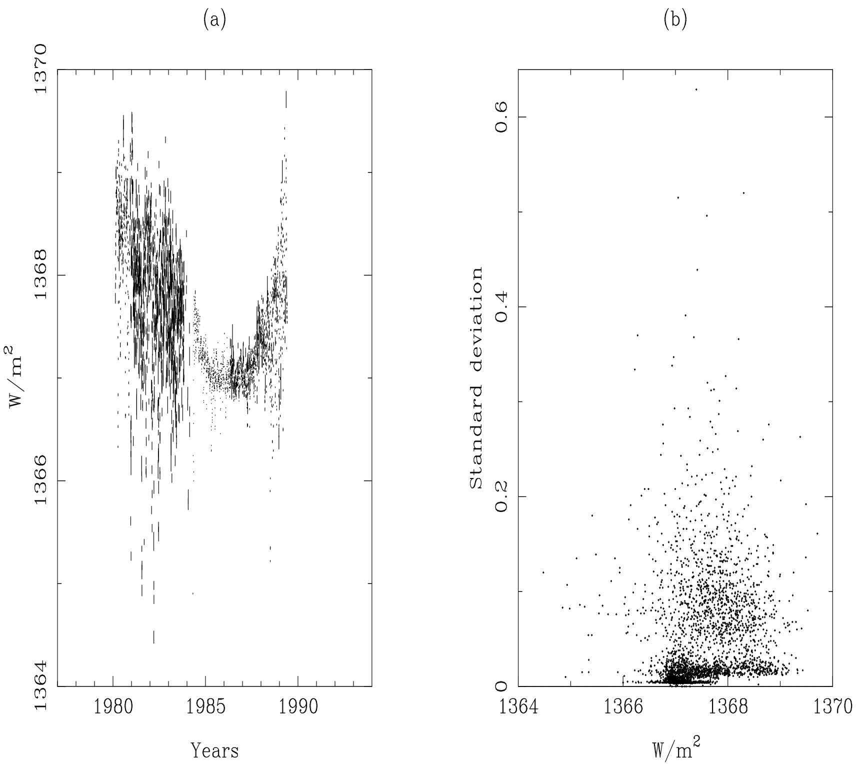

Fig. 1. The daily mean values of the SMM/ACRIM I total solar irradiance are plotted (a). Each data point represents the daily mean values; the associated vertical bars represent the standard deviations of the daily means ($\pm 1\sigma$). The standard deviations versus the daily ACRIM I total irradiance data are given in (b).

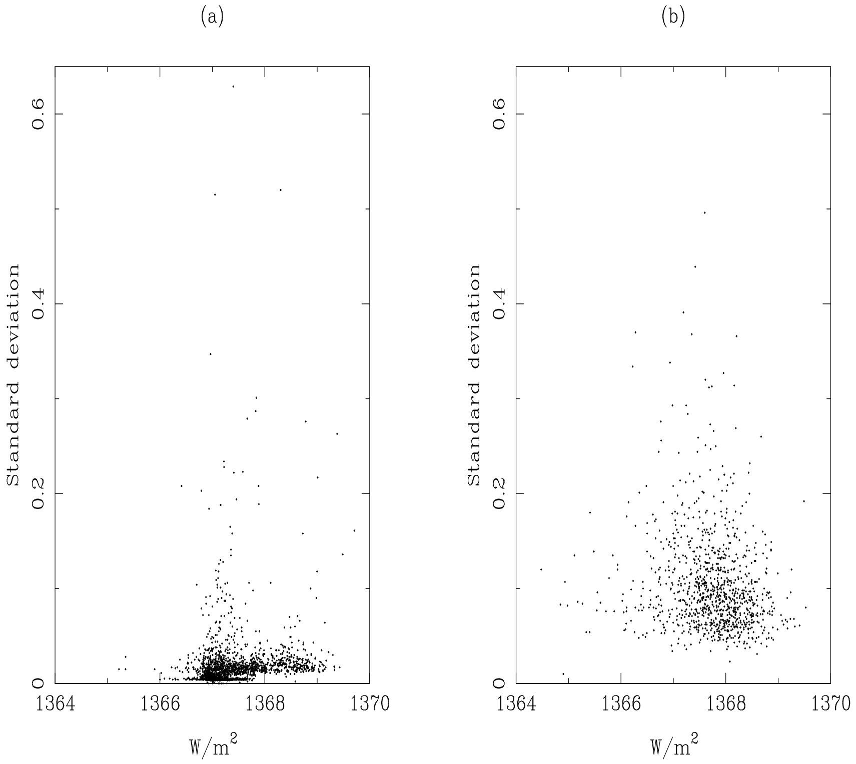

Fig. 2. The standard deviations of the ACRIM I data versus the daily irradiance values during the normal operational mode of the satellite (from February to December 1980 and from May 1984 to June 1989) are plotted in (a); the same is shown for the spin operational mode (from December 1980 to May 1984) (b).

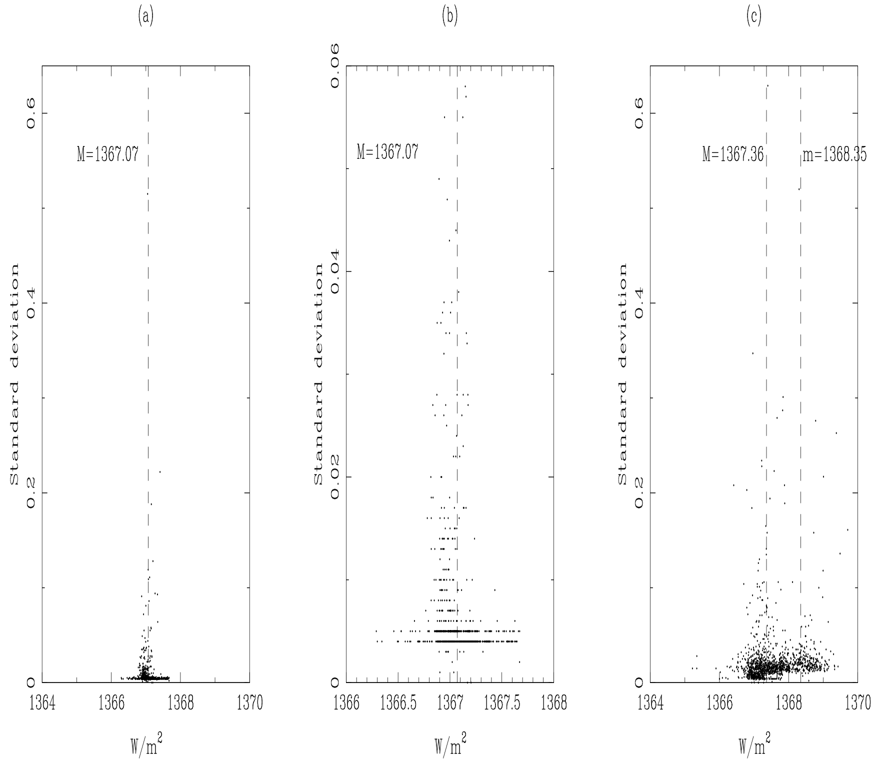

Fig. 3. The standard deviations of the normal operational mode of ACRIM I data versus the daily quiet-Sun irradiance values (between July 1, 1984 and September 30, 1986) are given in (a). In (b), the plot indicates the same data with STD less than 0.06 W/m^2. (c) shows the STD against the daily active-Sun irradiance values (for the time interval of February to December 1980 and October 1, 1986 to June 2, 1989). The vertical lines represent the mean irradiance values, for the rising portion of solar cycle 22 from October 1, 1986 (M = 1367.36 W/m^2) and for 1980, the maximum of solar cycle 21 (m = 1368.35 W/m^2), respectively.

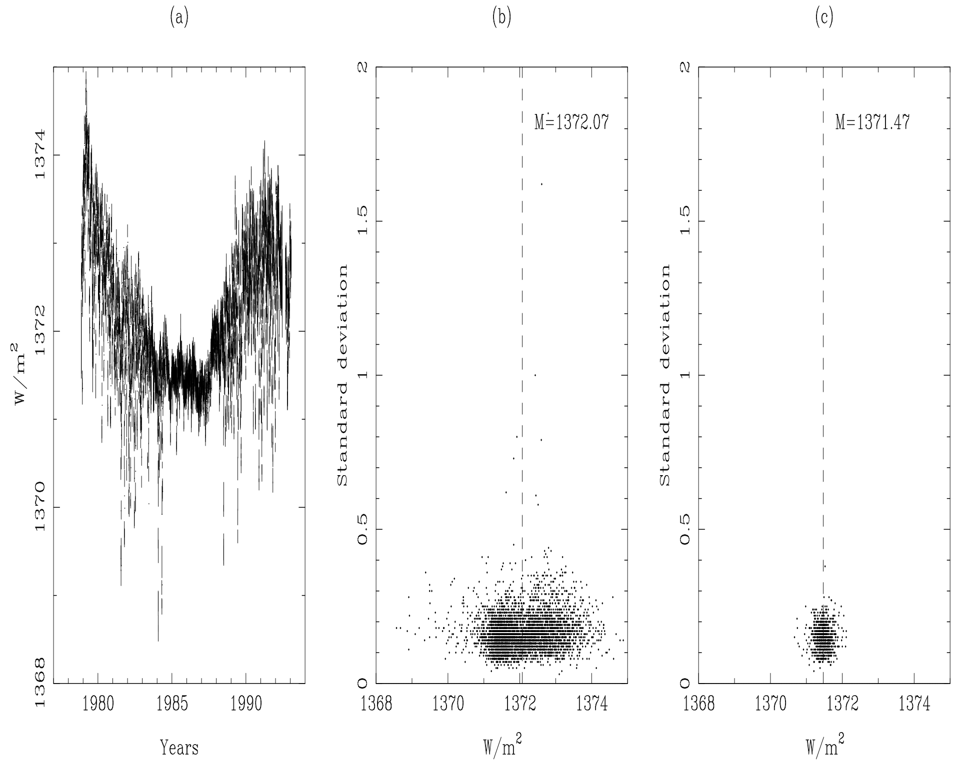

Fig. 4. The daily mean values of the Nimbus-7/ERB total irradiance with their standard deviations are presented in (a). The corresponding scatter plot diagram between the STD and irradiance values is plotted in (b). The scatter plot in (c) represents the minimum of solar cycle 21.

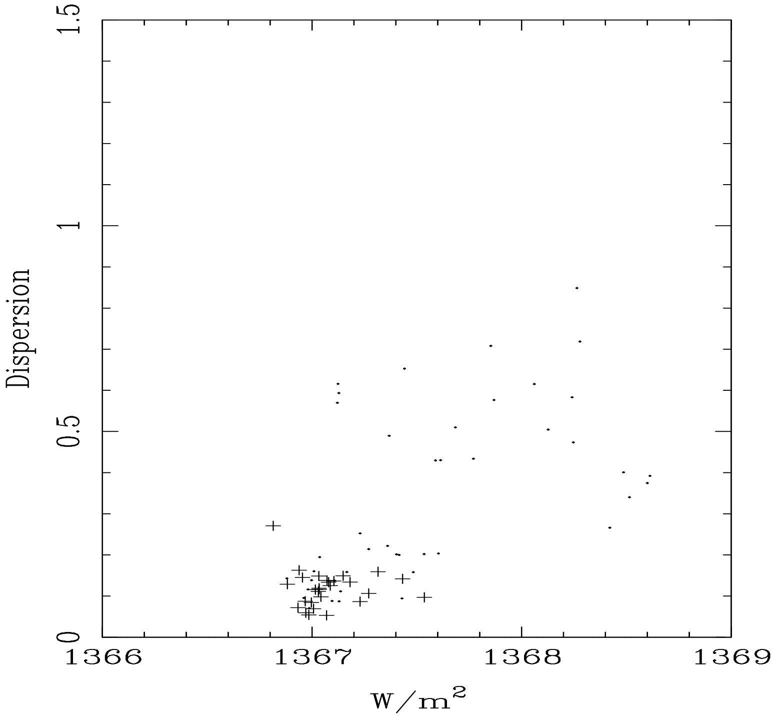

Fig. 5. The dispersion values against the monthly means of the ACRIM I total irradiance. The crosses represent the minimum of solar cycle 21, whereas the dots refer to solar maximum activity in 1980 and the increasing solar activity conditions from October 1986 to June 1989.

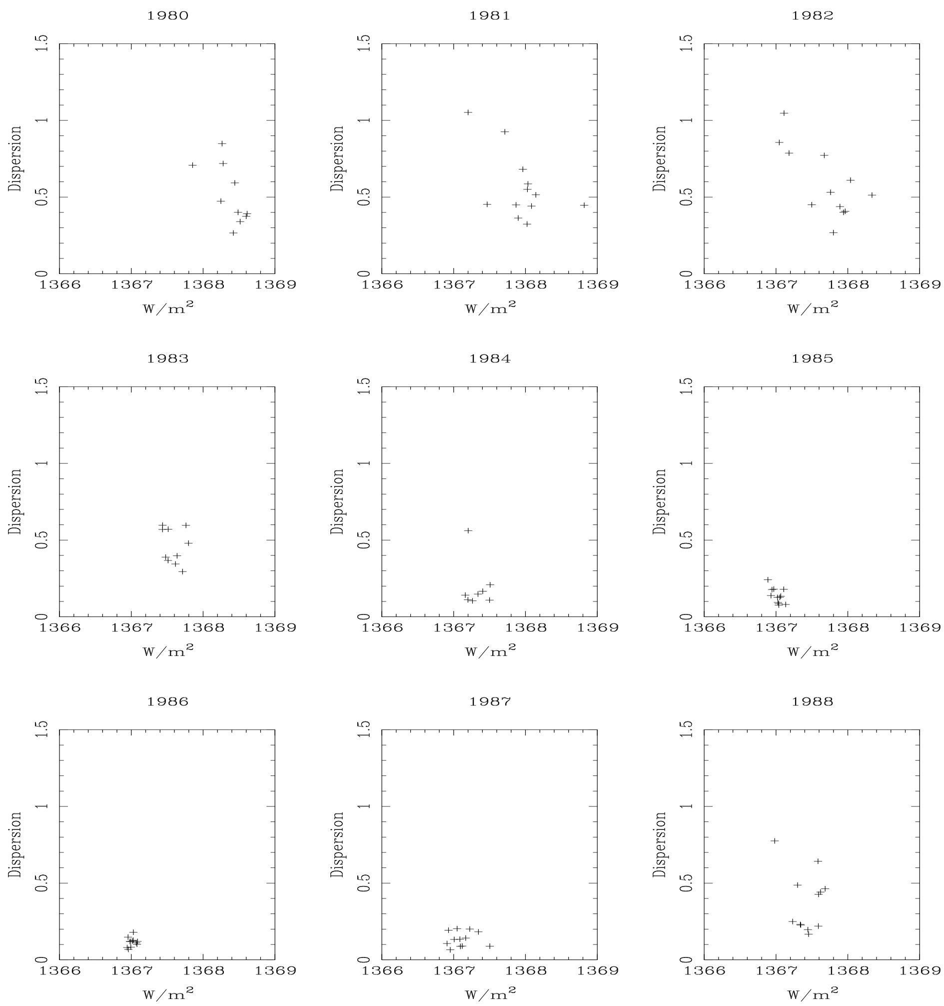

Fig. 6. The yearly ACRIM I total solar irradiance dispersion diagrams between 1980 and 1989.

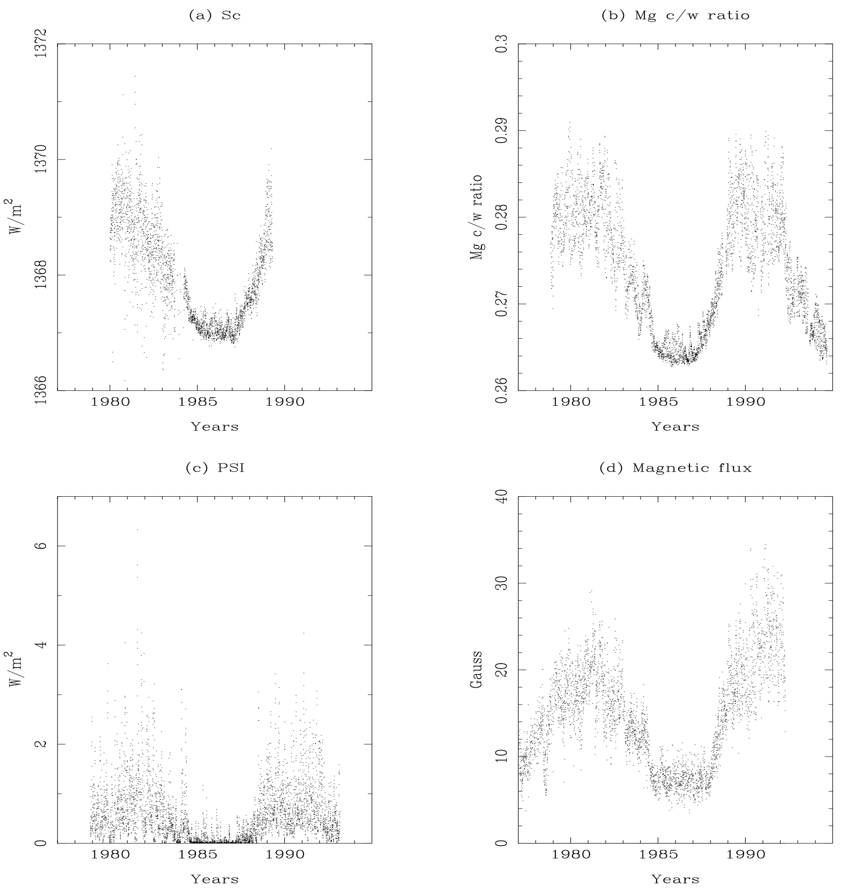

Fig. 7. Time series of the ACRIM I + PSI (a), combined Nimbus-7/NOAA9 Mg c/w ratio (b), PSI (c), and the full disk magnetic flux (d).

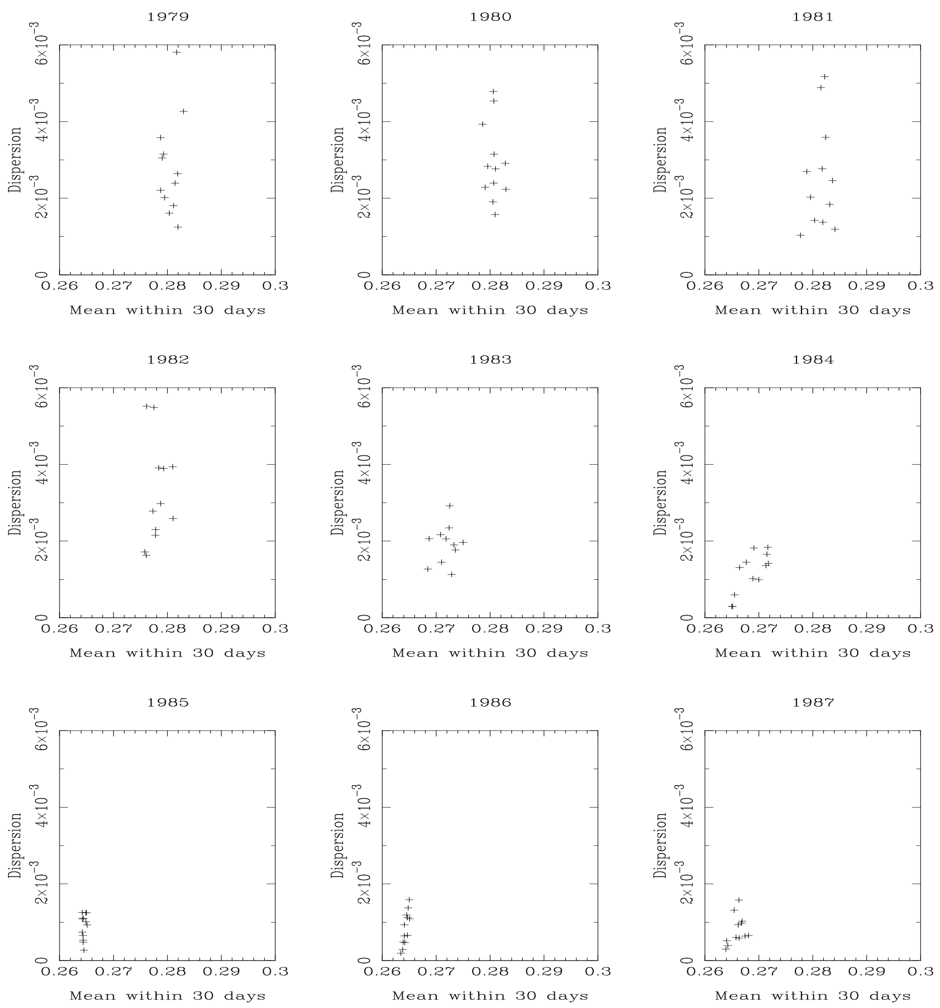

Fig. 8. The yearly Mg c/w ratio dispersion diagrams (from 1979 to 1987).

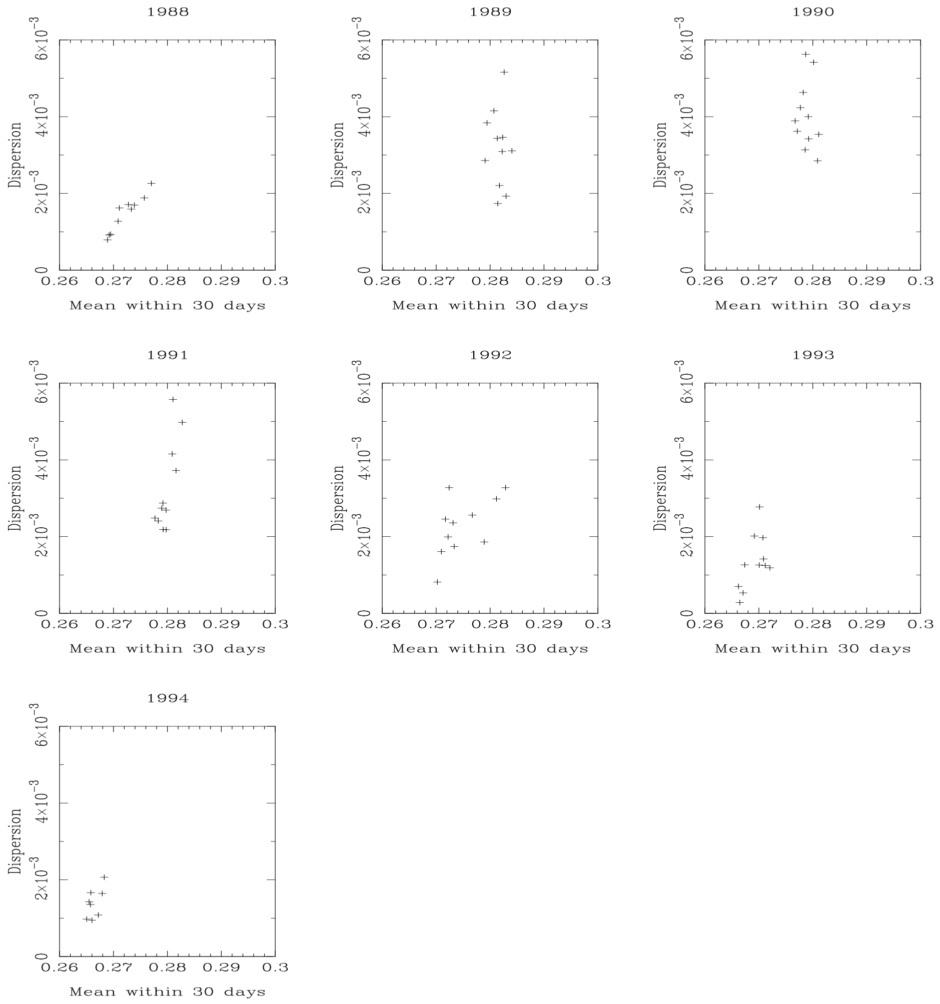

Fig. 9. The yearly Mg c/w ratio dispersion diagrams (from 1988 to 1994).

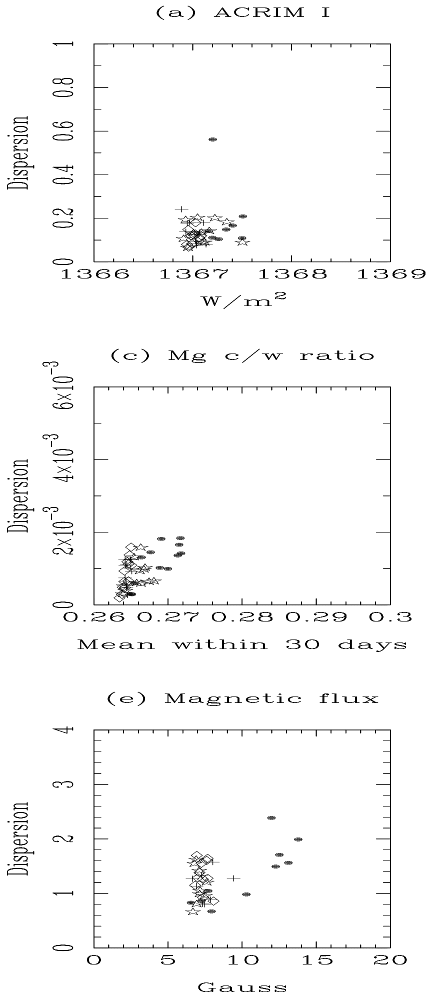

Fig. 10. Dispersion diagrams for ACRIM I (a), S_c (b), Mg c/w ratio (c), PSI (d) and the full disk magnetic flux (e) for minimum solar activity conditions. The dots represents data for 1984, crosses for 1985, diamonds for 1986 and stars for 1987.

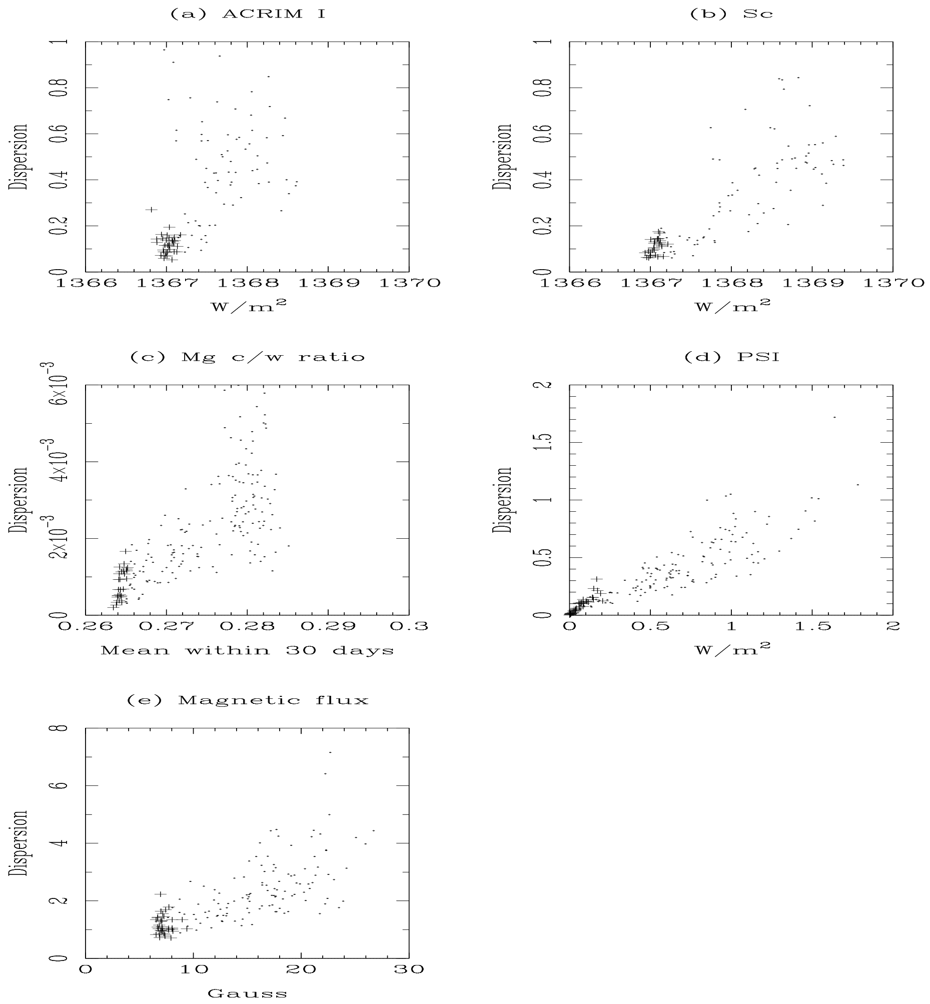

Fig. 11. Dispersion diagrams for ACRIM I (a), S_c (b), Mg c/w ratio (c), PSI (d) and the full disk magnetic flux (e) For each figure the cloud of cross corresponds to the minimum of the cycle 21, as defined in Table II, the cloud of points corresponds to the active phase of the Sun.